QUANTUM TRANSPORT IN INHOMOGENEOUS MULTI-WALL NANOTUBES

S. Sanvito[1,2,3], Y.-K. Kwon[3], D. Tománek[3], and C.J. Lambert[1]

[1]*School of Physics and Chemistry, Lancaster University, Lancaster, LA1 4YB, UK*
[2]*DERA, Electronics Sector, Malvern, Worcs. WR14 3PS, UK*
[3]*Department of Physics and Astronomy, and Center for Fundamental Materials Research, Michigan State University, East Lansing, Michigan 48824-1116*

INTRODUCTION

Carbon nanotubes[1,2] are narrow seamless graphitic cylinders, which show an unusual combination of a nanometer-size diameter and millimeter-size length. This topology, combined with the absence of defects on a macroscopic scale, gives rise to uncommon electronic properties of individual single-wall nanotubes[3,4], which depending on their diameter and chirality, can be either metallic, semiconducting or insulating[5–7].

In this paper we focus attention only on metallic nanotubes and in particular on the so-called "armchair" nanotubes. An armchair nanotube is a graphite tube in which the hexagon rows are parallel to the tube axis. If n is the number of carbon dimers along the nanotube circumference the tube will be labeled as (n, n) nanotube. One of the most important properties of the armchair nanotubes is that they behave like a mono-dimensional metal and this is directly connected with their structure. The electronic wave-length in fact is quantized around the circumference of the tube because of the periodic boundary conditions. This gives rise to mini-bands along the tube axis and the tube is metallic or insulating whether or not one or more mini-bands cross the Fermi energy. In the case of armchair nanotubes two mini-bands along the tube axis cross the Fermi energy[8], therefore, according to scattering theory[9], the conductance is expected to be $2G_0$, where $G_0 = 2e^2/h \approx (12.9\ \mathrm{k}\Omega)^{-1}$ is the quantum conductance. Direct evidence of the de-localization of the wave function along the tube axis has been already shown[10,11], while a direct measurement of the conductance quantization for single-wall nanotubes is still missed (for an introduction to electronic transport in carbon nanotubes see reference 12).

The situation for multi-wall nanotubes is rather different. A multi-wall nanotube consists of several single-wall nanotubes inside one another, forming a structure reminiscent of a "Russian doll". A section of a double-wall (5,5)@(10,10) armchair nanotube is presented in figure 1.

Recent measurements[13] of the conductance in multi-wall nanotubes have raised a significant controversy due to the observation of unexpected conductance values and of ballistic transport at temperatures far above room temperature. In these experiments

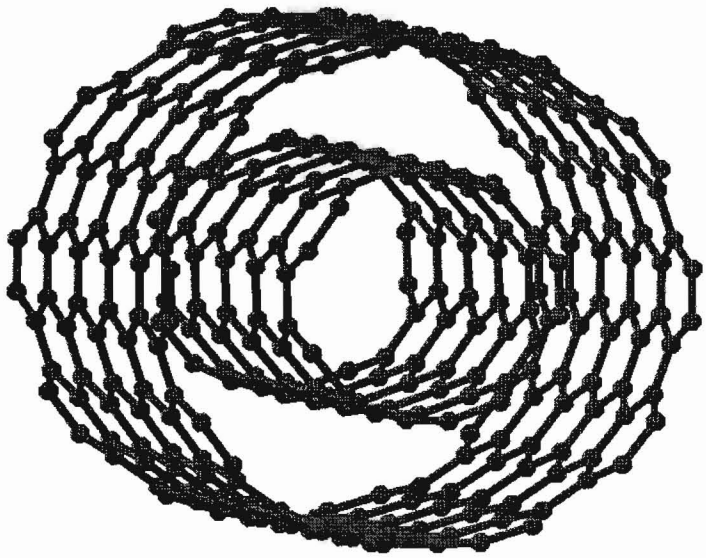

Figure 1: Section of a (5,5)@(10,10) "armchair" nanotube.

several multi-wall nanotubes are glued to a gold tip, which acts as the first electrode, with a colloidal silver paint. The second electrode is made by a copper bowl containing mercury, which provides a gentle contact with the nanotube. The tip is lowered into the mercury and the two-probe conductance is measured as a function of the immersion depth of the tubes into the mercury. The main feature of the experiments is that at room temperature the conductance shows a step-like dependence on the immersion depth, with a value of $0.5\,G_0$ for low immersion and $1\,G_0$ when the tip is further lowered. The value of $0.5\,G_0$ usually persists for small immersion depths ($\leq$ 40nm) and is completely absent in some samples, while the value $1\,G_0$ is found for very long immersion depths, up to 0.5μm. Nevertheless some anomalies have been found with conductances of $0.5\,G_0$ lasting for more than 500nm[13].

While the ballistic behavior up to high temperature can be explained by the almost complete absence of backward scattering[14], the presence of such conductance values is still not completely understood. In the absence of inter-tube interactions, if one assumes that m of the nanotubes forming the multi-wall nanotube are metallic and in contact with both the electrodes, then a conductance of $2mG_0$ is expected for the multi-wall nanotube. This means that even in the extreme case in which only one tube is metallic and in contact with the electrodes a conductance of $2G_0$ must be measured. Therefore the values $0.5\,G_0$ and $1\,G_0$ are largely unexpected. One possible explanation, provided by the authors of the experiments, is that only the outermost tube is responsible for the transport and that the anomalous conductance is the result of scattering to impurities. Nevertheless both these hypothesis may be challenged. The first is based on the assumption that, since mercury does not wet the innermost tubes, it does not provide an efficient electrical contact with the innermost part of the multi-wall nanotube. This may not be the case because the interaction between the different walls may be large and the motion of electrons across the structure efficient. As far as the second hypothesis concerns, it has been shown recently[15] that disorder averages over the tube's circumference, leading to an electron mean free path that increases with the nanotube diameter. Therefore single impurities affect transport only

weakly, particularly in the nanotube forming the outermost shell, which has the largest diameter.

In this paper we address these puzzling measurements and show that the structural properties of multi-wall nanotubes can explain their peculiar transport. The electronic band structure of multi-wall carbon nanotubes[16–18], as well as single-wall ropes[19,20] is now well documented. More recently, it has been shown that pseudo-gaps form near the Fermi level in multi-wall nanotubes[18] due to inter-wall coupling, similar to the pseudo-gap formation in single-wall nanotube ropes[19,20]. Here we demonstrate that the unexpected transport properties of multi-wall nanotubes arise from the inter-wall interaction. This interaction may not only block some of the quantum conductance channels, but also redistribute the current non-uniformly over the individual tubes. When only the outermost tube is in contact with one of the voltage/current electrodes, then this forms a preferred current path and, because of inter-tube interaction, the conductance of the whole system will typically be smaller than $2G_0$.

The paper is organized as follows. In the next section we will briefly describe a general scattering technique to compute the transport properties of finite systems attached to semi-infinite contacts, both described by a tight-binding Hamiltonian. In the following section we will discuss the transport in infinite multi-wall nanotubes and understand which are the effects of the inter-tube interaction both on the dispersion and on the wave-function of the tube. Then we present the results for transport properties of inhomogeneous multi-wall nanotubes, giving an explanation of the experiments of reference 13. In this part we will consider different scenarios about the structure of the electrical contacts. At the end we will make some final remarks.

GENERAL SCATTERING TECHNIQUE

To determine transport properties of finite multi-wall nanotubes, we combine for the first time, a tight-binding parameterization determined by *ab-initio* calculations for simpler structures[21], with a scattering technique developed recently for magnetic multilayers[22,23]. The use of a tight-binding model is justified by the necessity to deal with a system comprising a large number of degrees of freedom. This parameterization has been used to describe detailed electronic structure and total energy differences of systems with unit cells which are too large to handle accurately by *ab-initio* techniques. The electronic structure and superconducting properties of the doped C_{60} solid[24], the opening of a pseudo-gap near the Fermi level in a rope consisting of (10,10) nanotubes[20] and in (5,5)@(10,10) double-wall nanotubes[18] are some of the problems successfully tackled by this technique. The band structure energy functional is augmented by pairwise interactions describing both the closed-shell interatomic repulsion and the long-range attractive van der Waals interaction. This reproduces correctly the interlayer distance and the C_{33} modulus of graphite. Independent checks of this approach can be carried out by realizing that the translation and rotation of individual tubes are closely related to the shear motion of graphite. We expect that the energy barriers in tubes lie close to the graphite value which, due to the smaller unit cell, is easily accessible to *ab-initio* calculations[25].

The scattering technique that we used have been recently employed in studies of giant magnetoresistance[22,23] and ferromagnetic/superconductor structures[26]. It yields the quantum-mechanical scattering matrix S for a phase-coherent system attached to external reservoirs. The rôle of the reservoirs is to inject and collect incoherent electrons into the scattering region. The energy-dependent conductance $G(E)$ in the

zero-temperature limit is computed by evaluating the Landauer-Büttiker formula[27]

$$G(E) = \frac{2e^2}{h} T(E) \,, \tag{1}$$

where $T(E)$ is the total transmission coefficient evaluated at the energy E (E_F in the case of zero-bias). The formula of equation (1) provides an exact relation between the conductance of a system and its scattering properties.

The transmission coefficient is evaluated using a scattering technique that combines a real space Green function calculation for the incoherent leads and a Gaussian elimination (ie "decimation") algorithm for the scattering region. A general scheme of the technique is presented in figure 2, where we indicate how a transport problem can be mapped onto a quantum mechanical scattering problem.

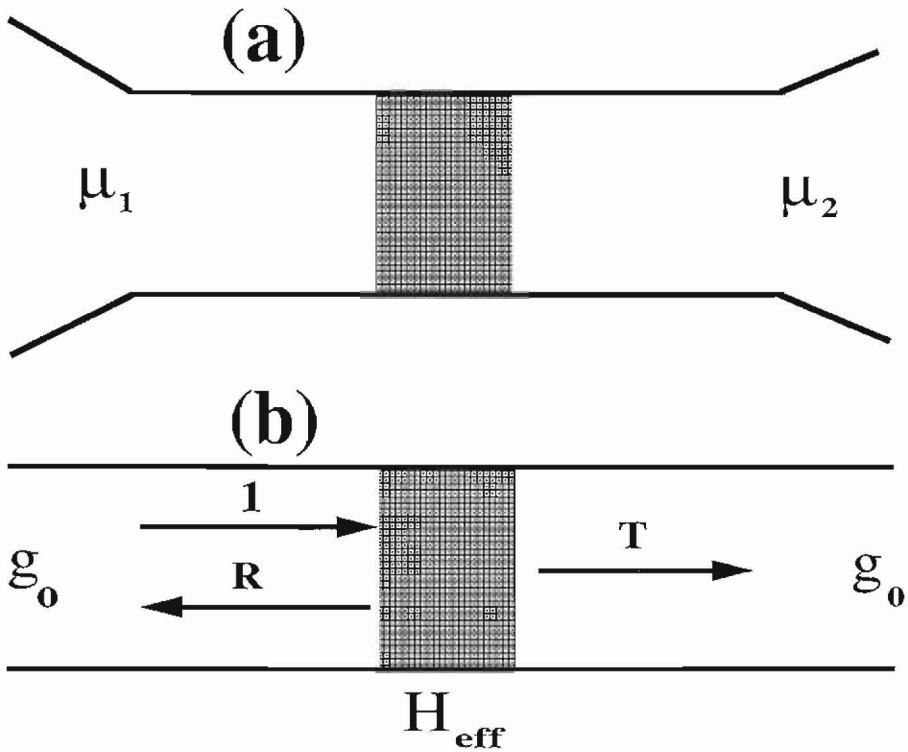

Figure 2: Scheme of the scattering calculation. The system (a) consists in two reservoirs with chemical potentials μ_1 and μ_2 separated by a scattering region. The problem is mapped by using the Landauer-Büttiker formalism onto a quantum mechanical scattering problem (b). The incoming scattering channels in the leads are calculated through the surface Green function g_0. The effective coupling matrix H_{eff} is computed by "decimating" the internal degrees of freedom of the scattering region. The total transmission T and reflection R coefficients are then calculated by solving exactly the Dyson's equation and by using a generalization of the Fisher-Lee relations.

Suppose the total Hamiltonian H for the whole system (nanotubes plus external leads) can be written

$$H = H_{\text{L}} + H_{\text{L-NT}} + H_{\text{NT}} + H_{\text{NT-R}} + H_{\text{R}} \,, \tag{2}$$

where H_{L} and H_{R} describe respectively the semi-infinite left-hand side and right-hand side lead, $H_{\text{L-NT}}$ and $H_{\text{NT-R}}$ are the coupling matrices between the leads and the nanotube and H_{NT} is the Hamiltonian of the nanotube. In what follows we will consider the leads themselves to be carbon nanotubes, whose number of walls depends on the position of the electrical contacts. This is justified when the transport bottleneck is

formed by the nanotubes and not to the metal-nanotube contacts. As far as we know detailed *ab-initio* analysis of metal/nanotube interaction is still not available.

The surface Green function $g_0^{\rm S}$ of the leads are calculated by numerically evaluating the general semi-analytic formula given in reference 22. One of the key-points of such a calculation is to compute the scattering channels in the leads. Suppose z to be the direction of the transport and the Hamiltonian of the leads to be an infinite matrix of trigonal form with respect to such a direction, with the matrices H_0 and H_1 respectively in the diagonal and off-diagonal positions. Therefore the dispersion relation for electrons in a Bloch state

$$\psi_z = \frac{1}{v_k^{1/2}} e^{ikz} \phi_k \tag{3}$$

and moving along z with unit flux can be written as

$$(H_0 + H_1 e^{ik} + H_{-1} e^{-ik} - E)\phi_k = 0 \,, \tag{4}$$

where v_k is the group velocity corresponding to the state (3) and $H_{-1} = H_1^\dagger$ ($H_0 = H_0^\dagger$). Note that the matrices H_0 and H_1 describe respectively the interaction within a unit cell and the interaction between adjacent cells. If a unit cell possesses M degrees of freedom, these matrices will be $M \times M$ matrices. Moreover ϕ_k is a M dimensional column vector which describes the transverse degrees of freedom of the Bloch-function. The Green function in the leads is constructed by adding up states of the form of equation (3) with k both real and imaginary, which means that the dispersion relation (4) must be solved for real energies in the form $k = k(E)$. This is the opposite to what is usually computed by ordinary band structure theory where one is interested in finding all the real energies $E = E(k)$ for a chosen real k-vector. Moreover in the calculation of $k = k(E)$ instead of solving the equation

$$\det\left(H_0 + H_1 e^{ik} + H_{-1} e^{-ik} - E\right) = 0 \,, \tag{5}$$

which involves the use of a root tracking algorithm in the complex plane, we map the problem onto an eigenvalue problem by defining the matrix $\mathcal{H}$

$$\mathcal{H} = \begin{pmatrix} -H_1^{-1}(H_0 - E) & -H_1^{-1} H_{-1} \\ \mathcal{I} & 0 \end{pmatrix} \,, \tag{6}$$

where $\mathcal{I}$ is the $M \times M$ identity matrix. The eigenvalues of $\mathcal{H}$ are the roots e^{ik} and the upper half of the eigenvectors of $\mathcal{H}$ are the corresponding eigenvectors ϕ_k.

The second part of the calculation involves computing an effective coupling matrix between the surfaces of the scattering region. Note that the purpose of a scattering technique is to calculate the S matrix between electrons in the leads. Therefore one is not interested in information regarding the internal degrees of freedom of the scattering region, but only in the resulting coupling between the external interfaces. This can be achieved by reducing the matrix $H_{\rm L-NT} + H_{\rm NT} + H_{\rm NT-R}$ to an effective coupling matrix $H_{\rm eff}$. Suppose the total number of degrees of freedom of the Hamiltonian $H_{\rm L-NT} + H_{\rm NT} + H_{\rm NT-R}$ is N, and the number of degrees of freedom of the lead surfaces M. One can eliminate the $i = 1$ degree of freedom (not belonging to the external surfaces) by reducing the $N \times N$ total Hamiltonian to an $(N-1) \times (N-1)$ matrix with elements

$$H_{ij}^{(1)} = H_{ij} + \frac{H_{i1} H_{1j}}{E - H_{11}} \,. \tag{7}$$

Repeating this procedure l times we obtain the "decimated" Hamiltonian at l-th order

$$H_{ij}^{(l)} = H_{ij}^{(l-1)} + \frac{H_{il}^{(l-1)} H_{lj}^{(l-1)}}{E - H_{ll}^{(l-1)}} \,, \tag{8}$$

and finally after $N - M$ times, the effective Hamiltonian

$$H_{\text{eff}}(E) = \begin{pmatrix} H^*_{\text{L}}(E) & H^*_{\text{LR}}(E) \\ H^*_{\text{RL}}(E) & H^*_{\text{R}}(E) \end{pmatrix} . \tag{9}$$

In the equation (9) the matrices $H^*_{\text{L}}(E)$ and $H^*_{\text{R}}(E)$ describe the intra-surface couplings respectively in the left-hand side and right-hand side surfaces, and $H^*_{\text{LR}}(E)$ and $H^*_{\text{RL}}(E)$ describe the effective coupling between these surfaces. From the above equations it is clear that only matrix elements coupled to the eliminated degree of freedom are redefined. This exact recursive technique therefore turns out to be very efficient in the case of short-range interaction like the nearest neighbors tight-binding model considered here. Two important considerations must be made. Firstly we note that both the Green function calculation and the "decimation" require a fixed energy. Once this has been set the calculation is exact and does not use any approximation. Secondly the calculation of the Green function is completely decoupled by the calculation of the effective Hamiltonian for the scatterer. This can allow very efficient numerical optimizations, particularly in the study of disordered systems[28].

Once both the surface Green function of the leads g^{S}_0 and the effective coupling Hamiltonian $H_{\text{eff}}(E)$ are computed then the total Green function G^{S} for the whole system (leads plus scattering region) are easily calculated by solving the Dyson's equation

$$G^{\text{S}}(E) = [(g^{\text{S}}_0(E))^{-1} - H_{\text{eff}}]^{-1} . \tag{10}$$

Finally the scattering matrix elements are extracted from G^{S} by using a generalization of the Fisher-Lee relations[29].

For the case of leads made by carbon nanotubes a final observation must be considered. The unit cell along the axis of the nanotube comprises two atomic planes, and since the hopping matrix between sequential unit cells H_1 is therefore singular, the dispersion relation cannot be calculated by using the equation (6). We avoid this complication by projecting out the non-coupled degrees of freedom between sequential cells before calculating the scattering channels. This has been done by using the "decimation" technique described above.

CONDUCTANCE IN MULTI-WALL NANOTUBES

For an homogeneous system $T(E)$ assumes integer values corresponding to the total number of open scattering channels at energy E. For individual (n, n) "armchair" tubes, this integer is further predicted to be even[8], with a conductance of $2G_0$ near the Fermi level. As an example, our results for the conductance $G(E)$ and the density of states of the $(10, 10)$ nanotube are shown in Fig. 3.

The main feature of an "armchair" nanotube is its true mono-dimensional metallic behavior. Note that the density of state shows mono-dimensional van Hove singularities which are due to the presence of dispersion-less mini-bands. This is reflected in the energy-dependent conductance which shows a typical step-like behavior. Such steps appear whenever the energy crosses a new mini-band, and therefore correspond to the van Hove singularities in fig 3a. It is crucial to note that in an infinite system every scattering channel gives the same contribution G_0 to the conductance independently from its dispersion and group velocity. The situation is rather different in an inhomogeneous system, where the scattering of electrons from low dispersion to high dispersion bands of different materials, can give rise to strong backward scattering and therefore

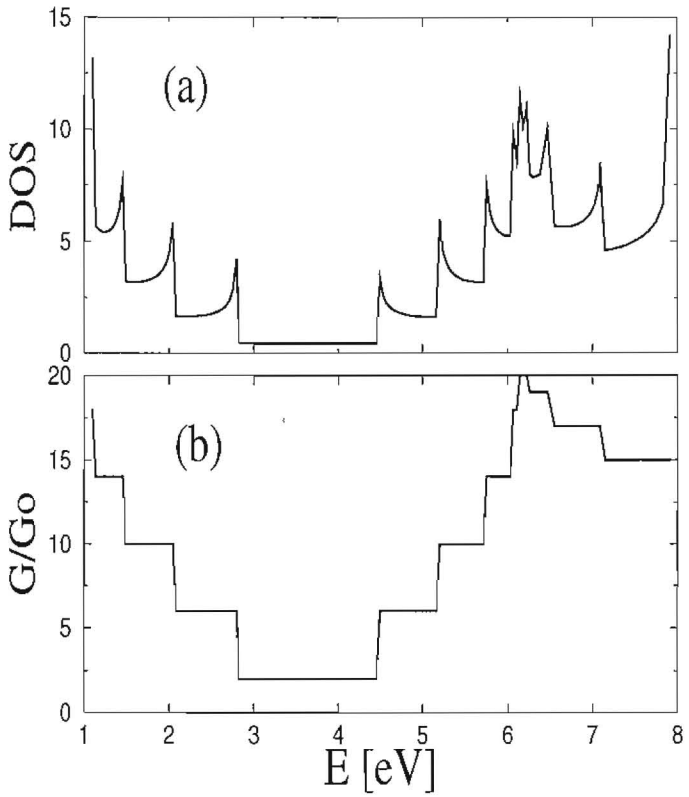

Figure 3: Single-wall (10,10) nanotube. (a) Local density of states. (b) Conductance as a function of energy. The Fermi level lies at 3.65 eV.

to a reduction of the conductance[22,23,28]. At the Fermi energy of an "armchair" nanotube (in this case $E_F = 3.65$ eV) only two scattering channels are present resulting in a conductance $2G_0$, which remains constant in an energy interval of approximately 1.5eV.

Consider now multi-wall nanotubes. As observed in the introduction, in the absence of inter-tube interactions, different tubes behave as conductors in parallel and the conductances are simply additive. Therefore, since the position of the Fermi energy does not change with the tube diameters we expect a conductance $2mG_0$ for a multi-wall nanotubes comprising m walls. Note also that the width of the energy region around the Fermi energy where the conductance is $2G_0$, depends only weakly on the tube diameters. The situation changes drastically when inter-tube interaction is switched on. In figures 4 and 5 we present the density of states and the conductance respectively for a (10,10)@(15,15) and for a (5,5)@(10,10)@(15,15) multi-wall nanotube.

In the figures we restricted the energy window to the region where the single-wall armchair nanotubes present conductances of $2G_0$. The main feature of both the figures is the presence of pseudo-gaps[18] which lower the conductance from the expected value $2mG_0$. In the case of a double-wall nanotube, this results in two regions where the conductance passes from $4G_0$ to $2G_0$, while in triple-wall nanotube the values $6G_0$, $4G_0$ and $2G_0$ are possible. Nevertheless both these results are still not consistent with the experimental observations of $1G_0$ and $0.5G_0$[13].

It is important to note that the presence of energy pseudo-gaps does not only lowers the conductance but also gives rise to two important effects. First it changes drastically the dispersion of the mini-bands close to the gaps. At the edge of the gaps in fact the dispersion passes from a linear to an almost dispersion-less parabolic-like structure. This is shown in figure 6 where we present the band structure along the

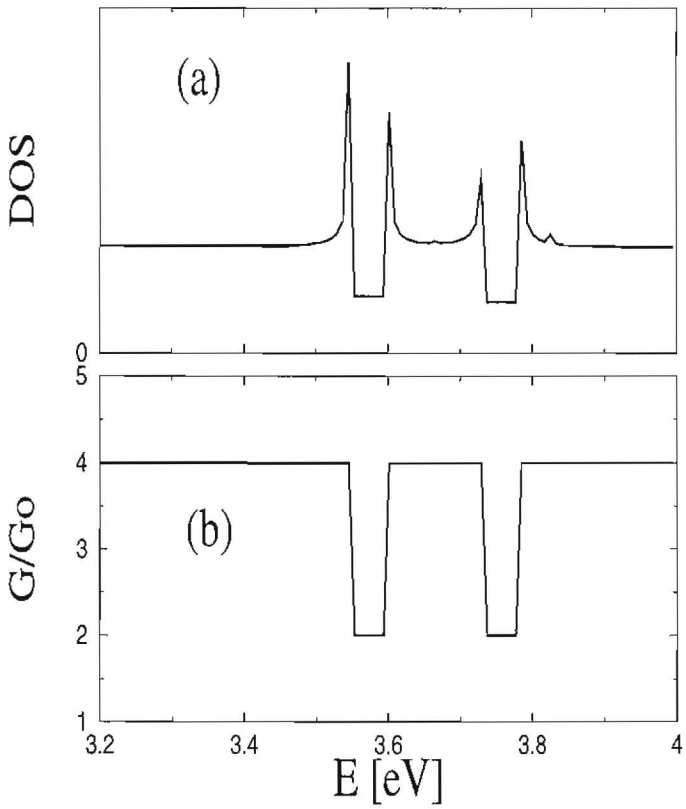

Figure 4: (a) Local density of states for a double-wall (10,10)@(15,15) nanotube. (b) Conductance as a function of energy.

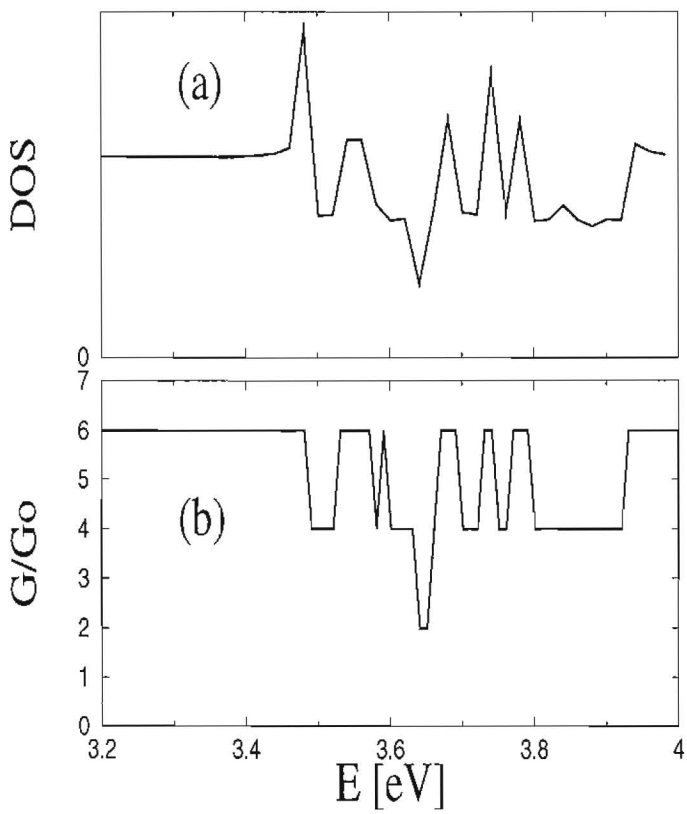

Figure 5: (a) Local density of states for a triple-wall (5,5)@(10,10)@(15,15) nanotube. (b) Conductance as a function of energy.

direction of the tube axis for a double-wall (10,10)@(15,15) nanotube (b) together with the band structure of a single-wall (15,15) nanotube.

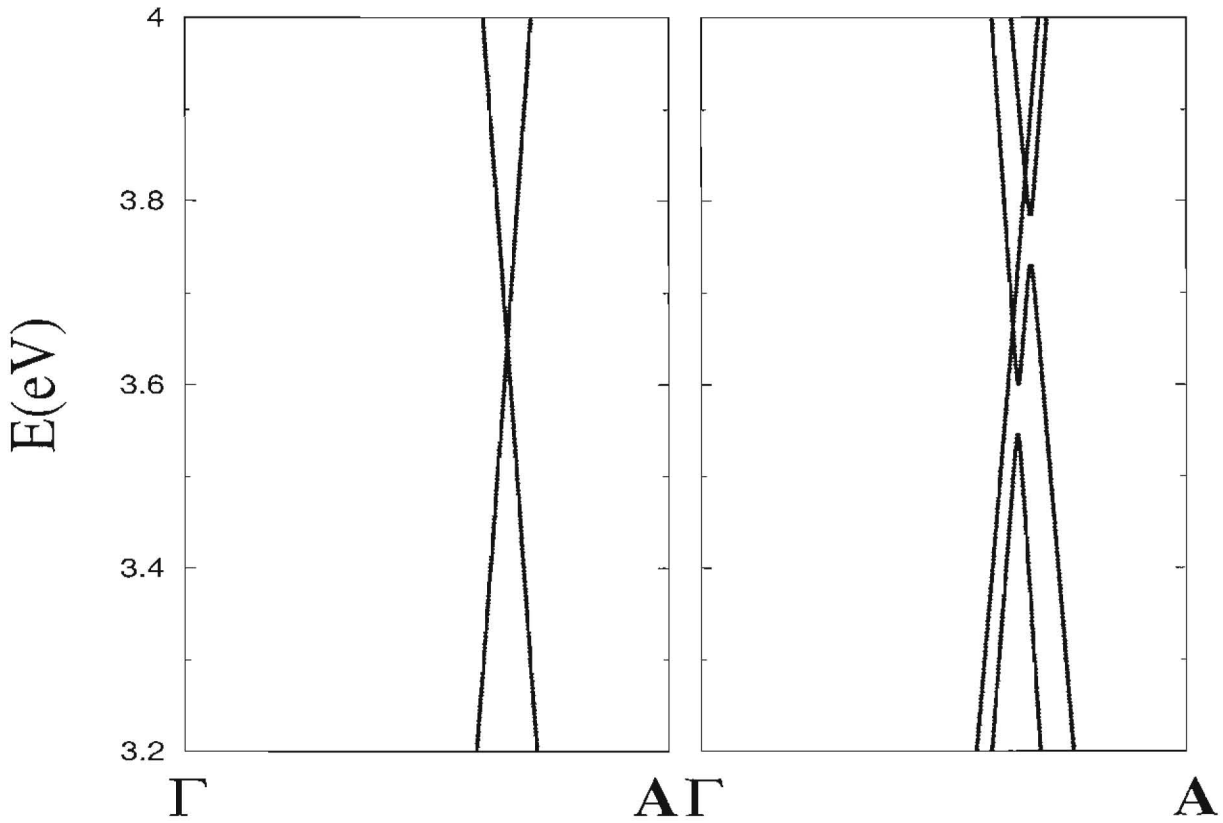

Figure 6: (a) Band structure along the tube axis for a (15,15) nanotube, with $E_F = 3.65$ eV. (b) Band structure along the tube axis for a (10,10)@(15,15) nanotube.

Secondly the amplitude of the wave-function across the nanotubes changes. Far from the gaps, where the effects of the inter-tube interaction are weak, the wave-function is expected to have a uniform distribution across the different walls composing the nanotube. This is what is found in the case of non-interacting walls, whereas in the vicinity of a pseudo-gap, the distribution changes dramatically and the amplitude may be enhanced along some walls and reduced along some others. To demonstrate this effect in figure 7 we present the partial conductance across the two walls composing a (10,10)@(15,15) nanotube and across the three walls composing a (5,5)@(10,10)@(15,15) nanotube. The partial conductance is defined as the projection of the total conductance for an infinite multi-wall tube onto the degrees of freedom describing the individual walls. From the figure it is very clear that the amplitude of the wave-function (which is proportional to the partial conductance) is not uniform across the structure and depends critically on the energy.

Both the change in the dispersion and the non-uniform distribution of the amplitude of the wave-function across the tubes have drastic effects on the transport of heterogeneous systems, because it creates strong inhomogeneities along the structure, and therefore strong backward scattering. This aspect, which occurs in a multi-wall nanotube when one of the innermost walls closes, will be discussed in the next section.

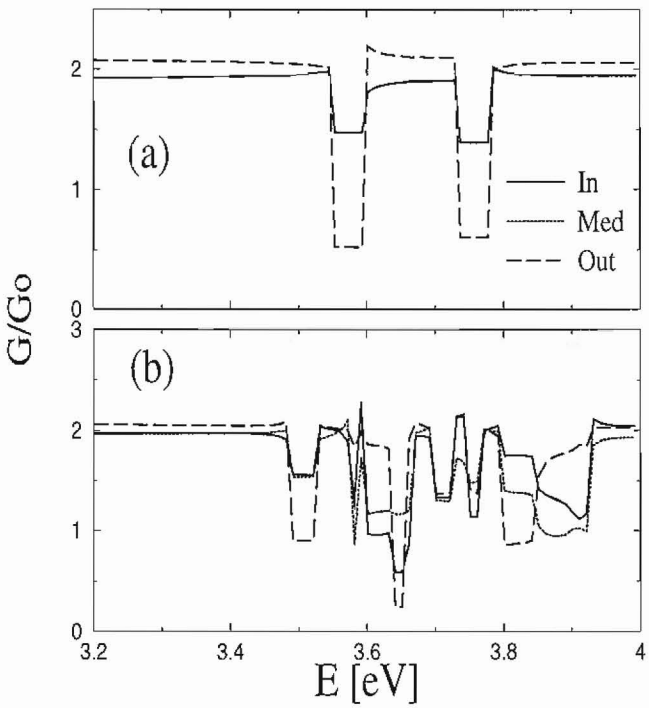

Figure 7: Partial conductance of (a) (10,10)@(15,15) and (b) (5,5)@(10,10)@(15,15) nanotube. The solid line, dotted and dashed lines represent the partial conductance respectively onto the innermost, the medium (only in the case of (5,5)@(10,10)@(15,15)) and the outermost tube. Note that within the pseudo-bandgaps the conductance does not distribute uniformly onto the different tubes.

TRANSPORT IN INHOMOGENEOUS MULTI-WALL NANOTUBES

In this section we will use the ideas developed above to describe the experiments of reference 13. Note that for inhomogeneous systems, where multi-wall nanotubes are contacted to the voltage/current probes, the conductance quantization in unit of $2G_0$ which we found also for multi-wall nanotube in presence of inter-wall interaction is evidently violated and fractional values of the conductance are allowed. One of the difficulties of the experiments, which use gold as one electrode and mercury as the other, is that not all tubes make contact with the electrodes. We have considered two different scenarios and have found that agreement with the experiments is obtained when we assume that only the outermost tube is in contact with the gold electrode, whereas the number of walls in contact with the mercury depends on the depth at which the tube is immersed into the liquid. This latter assumption may seem surprising, because the mercury does not wet the inner tubes. Nevertheless we believe that at equilibrium, the inter-tube interaction allows a uniform distribution of the chemical potential across the cross-section of the whole structure and therefore in the linear-response regime, the scattering problem reduces to a semi-infinite single-wall nanotube (the one in direct contact with gold) attached to a scattering region in which a variable number of walls are present (see fig.8a). Moreover a close analysis of the inter-tube matrix elements shows that these are of the same order of magnitude as the intra-wall ones. This means that electron transport between different walls may be efficient, as well as the electron feeding of the innermost walls from the electrons reservoirs.

Consider first the case in which only the outermost tube makes contact with the gold electrode. We argue that the step-like dependence of the conductance on the immersion depth is due to the fact that the scattering region makes contact with the

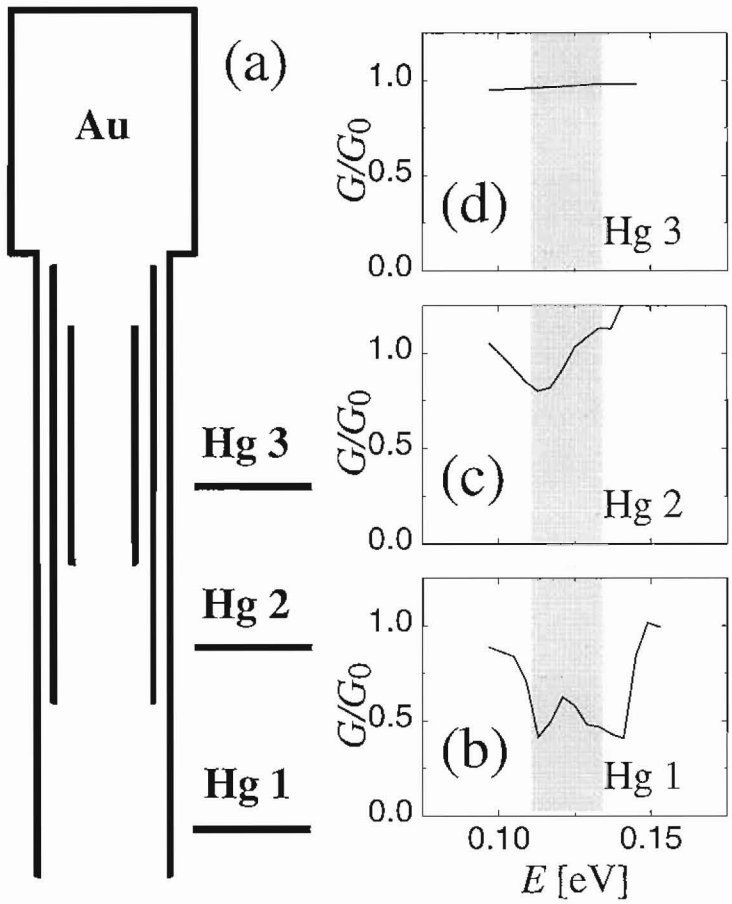

Figure 8: (a) Schematic geometry of the system in which only the outermost tube is contacted with the gold electrode for different immersion depths. (b)-(d) Conductance as a function of energy for the system of (a) at the immersion depths Hg1, Hg2, and Hg3. E is given with respect to E_F of the pristine (undoped) nanotube.

mercury reservoir via a multi-wall semi-infinite nanotube whose number of walls varies and depends on the immersion of the structure. For small immersion depths (such as Hg1 in fig.8a), only the outermost tube is in contact with mercury, because it is the only one with an end below the mercury level. A further lowering of the gold tip (to depths such as Hg2 and Hg3 in fig.8a) will sequentially place more inner walls into electrical contact with the mercury, thereby changing the conductance. We notice that the conductance of such a structure cannot be larger than that of the single-wall nanotube, which is the only tube in contact with the gold electrode.

In figure 8b we present the conductance as a function of energy for the inhomogeneous structure described in figure 8a. In all three cases, the simulated structure makes contact with the upper Au reservoir via a (15,15) nanotube, which forms the upper external lead, whereas the lower external lead contacting the Hg comprises either a single, double or triple-wall nanotube. The solid curve corresponds to a structure formed from a 200 atomic plane (AP) (5,5)@(10,10)@(15,15) triple-wall region, below which is attached to a 200 AP (10,10)@(15,15) double-wall region. The ends of the outer (15,15) nanotube are connected to semi-infinite (15,15) nanotubes, which form the external leads. The dashed curve corresponds to a structure formed from a 200 AP (5,5)@(10,10)@(15,15) triple-wall region. The upper end of the outer tube attached to a semi-infinite (15,15) nanotube, which forms the external lead contacting the Au reservoir. The lower end of the (10,10) and (15,15) nanotubes continue to infinity, and form a (10,10)@(15,15) external contact to the Hg reservoir. Finally the dot-dashed

line shows the conductance of a (5,5)@(10,10)@(15,15) nanotube, which at the lower end makes direct contact with the Hg and at the upper end, the outer tube continues to infinity, thereby forming a (15,15) external contact to the Au reservoir. These situations correspond to immersion of the tube into the mercury at positions Hg1, Hg2 and Hg3 respectively, where either one wall and two walls are in electrical contact with the mercury.

In all the simulations, the ends of the finite-length tubes are left open and we do not include capping layers. We believe that the capping layers are not crucial to the description of the transport properties of inhomogeneous multi-wall nanotubes, since these are mainly determined by the mis-match of wave-vectors between different regions. Figure 8b shows clearly that in an energy window of about 0.05eV (indicated by vertical dashed lines), the conductance for the first structure is approximately $0.5G_0$, while for the latter two is of order $1G_0$. Note that such energy window is two times larger than the bias used in the experiments and also much larger than room temperature. This suggests that these results are quite robust and will survives both at room temperature and moderate biases. This remarkable result is in excellent agreement with the recent experiments of reference 13.

The scattering in such an inhomogeneous structure arises from the reasons pointed out in the previous section. In the energy window considered in fact the infinite (5,5)@(10,10)@(15,15) presents a large pseudo-gap with conductance $4G_0$. We therefore expect that at both the interfaces of the (5,5)@(10,10)@(15,15) region with respectively the (10,10)@(15,15) region and the (15,15) tube, the mismatch of either the transverse components of the wave-function ϕ_k and the longitudinal k-vectors will be large. This gives rise to the strong suppression of the conduction observed in the experiments. In figure 9 we present the conductance as a function of immersion depth in mercury for the structure described above. The conductance is calculated at zero-temperature in the zero bias limit and the energy has been set in the middle of the marked region of figure 8a (3.825eV). Note again that the agreement with the curve of experiments of reference 13 is very good.

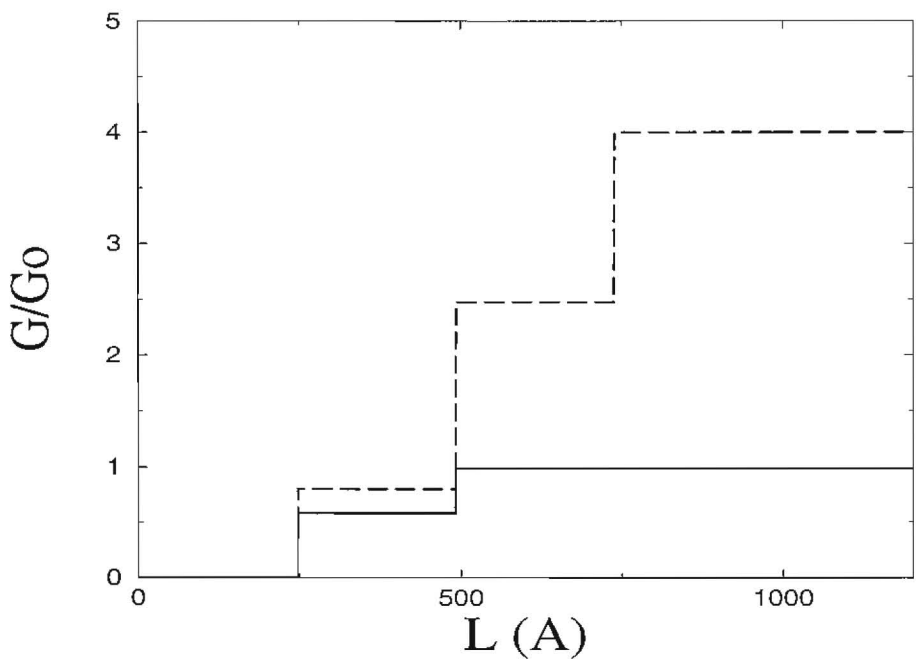

Figure 9: Conductance as a function of immersion depth. The solid curve corresponds to the structure of figure 8a and the dashed curve to that of figure 10a.

We now consider a second possible scenario, in which three tubes are in direct contact with the gold electrode. In this case the electrons are fed from gold into the structure directly along all the tubes. This contact can be simulated by a semi-infinite (5,5)@(10,10)@(15,15) nanotube with uniform chemical potential across the tubes. The structure considered is presented in figure 10a. In this case the upper bound of the conductance is no longer fixed by the single-wall tube to be $2G_0$ but can be as large as $6G_0$ and depends on the number of walls contacting the mercury. In figure 10b we show the conductance as a function of energy respectively for a 200 AP (10,10)@(15,15) nanotube sandwiched between a (15,15) and a (5,5)@(10,10)@(15,15) nanotube leads, for (10,10)@(15,15) nanotube lead in contact with a (5,5)@(10,10)@(15,15) nanotube lead, and for an infinite (5,5)@(10,10)@(15,15) nanotube. This again corresponds to the different levels of immersion Hg1, Hg2 and Hg3 in (Fig. 10a). Note that in the case in which the (5,5)@(10,10)@(15,15) nanotube is in direct contact with both the gold and the mercury electrodes its conductance corresponds to the number of opening scattering channels for the infinite triple-wall system.

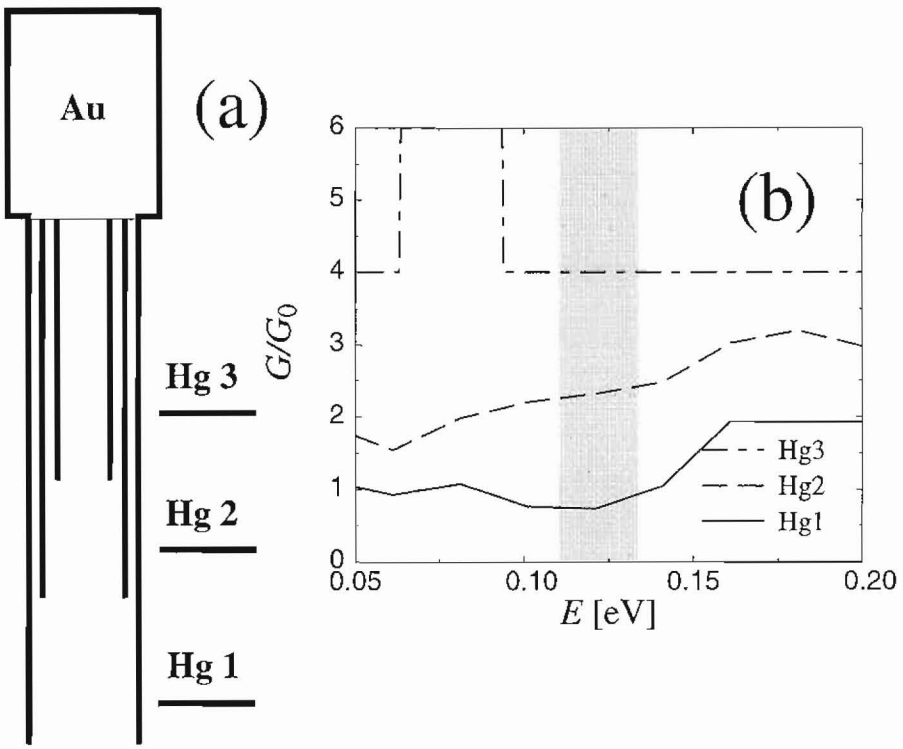

Figure 10: (a) Schematic geometry of the system in which three tubes tubes are contacted with the gold electrode for different immersion depths. (b) Conductance as a function of energy for the system of (a). E is given with respect to E_F of the pristine (undoped) nanotube.

Figure 10 shows that when all three tubes are electrically connected to the gold electrode, a much larger increase in the conductance occurs when a new wall is lowered below the mercury level, although this is still smaller than the value of $2G_0$, obtained for completely isolated tubes. In this case, corresponding to the different value of the immersion depth, we expect the conductance to be respectively $1G_0$, $2G_0$ and $4G_0$.

The large difference between the transport of the structures in figures 8a and 10a is therefore crucially dependent on the number of tubes which make a direct contact with the gold electrode. At the moment a complete description of the nanotube/metal interface is not available, although it will deserve further investigation both experimentally and theoretically.

CONCLUSIONS

To conclude we have presented a fully quantum scattering technique which yields the S matrix of inhomogeneous multi-wall nanotubes. We have shown that the inter-tube interaction drastically modifies transport, not only by opening pseudo-gaps close to the Fermi energy, but also by redistributing the amplitude of the transverse component of the wave-function across the multi-wall structure. These effects, when combined together, form a convincing explanation of puzzling experiments in which non-integer values of conductance have been found in multi-wall nanotubes[13]. To arrive at this quantitative description of the experiments, we have explored several possibilities regarding on the nature of the nanotube/metal interfaces. Only those calculations in which the outermost tube is in direct contact with the gold electrode showed good agreement with the experiments.

ACKNOWLEDGEMENTS

This work has been done in collaboration with the group of Prof. J.H. Jefferson at DERA Malvern, who is kindly acknowledged. SS acknowledges also the financial support by the DERA and the MSU-CMPT visitor fund. YKK and DT acknowledge financial support by the Office of Naval Research under Grant Number N00014-99-1-0252.

REFERENCES

1. S. Iijima, Nature **354**, 56 (1991).
2. For a general review, see M.S. Dresselhaus, G. Dresselhaus, and P.C. Eklund, *Science of Fullerenes and Carbon Nanotubes* (Academic Press Inc., 1996 San Diego), and references therein.
3. S. Iijima and T. Ichihashi, Nature **363**, 603 (1993).
4. D.S. Bethune, C.H. Kiang, M.S. de Vries, G. Gorman, R. Savoy, J. Vazquez, R. Beyers, Nature **363**, 605 (1993).
5. J.W. Mintmire, B.I. Dunlap, and C.T. White, Phys. Rev. Lett. **68**, 631 (1992).
6. R. Saito, M. Fujita, G. Dresselhaus, and M.S. Dresselhaus, Appl. Phys. Lett. **60**, 2204 (1992).
7. N. Hamada, S. Sawada, and A. Oshiyama, Phys. Rev. Lett. **68**, 1579 (1992).
8. L. Chico, L.X. Benedict, S.G. Louie and M.L. Cohen, Phys. Rev. B **54**, 2600 (1996), W. Tian and S. Datta, *ibid.* **49**, 5097 (1994), M.F. Lin and K.W.-K. Shung, *ibid.* **51**, 7592 (1995).
9. R. Landauer, Phil. Mag. **21**, 863 (1970).
10. S.J. Tans, M.H. Devoret, H. Dai, A. Thess, R.E. Smalley, L.J. Geerligs, C. Dekker, Nature **386**, 474 (1998).
11. M. Bockrath, D. H. Cobden, P. L. McEuen, N. G. Chopra, A. Zettl, A. Thess, R. E. Smalley Science **275**, 1922 (1997).
12. C. Dekker, Physics Today May 1999, 22 (1999).
13. S. Frank, P. Poncharal, Z.L. Wang, and Walt A. de Heer, Science **280**, 1744 (1998).
14. T. Ando, T. Nakanishi, J. Phys. Soc. Jpn. **67**, 1704 (1998).
15. C.T. White, T.N. Todorov, Nature **393**, 240 (1998).

16. Riichiro Saito, G. Dresselhaus, and M.S. Dresselhaus, J. Appl. Phys. **73**, 494 (1993).
17. Ph. Lambin, L. Philippe, J.C. Charlier, and J.P. Michenaud, Comput. Mater. Sci. **2**, 350 (1994).
18. Young-Kyun Kwon and David Tománek, Phys. Rev. B **58**, R16001 (1998).
19. P. Delaney, H.J. Choi, J. Ihm, S.G. Louie, and M.L. Cohen, Nature **391**, 466 (1998).
20. Young-Kyun Kwon, Susumu Saito, and David Tománek, Phys. Rev. B **58**, R13314 (1998).
21. D. Tománek and Michael A. Schluter, Phys. Rev. Lett. **67**, 2331 (1991).
22. S. Sanvito, C.J. Lambert, J.H. Jefferson, A.M. Bratkovsky, Phys. Rev. B **59**, 11936 (1999).
23. S. Sanvito, C.J. Lambert, J.H. Jefferson, A.M. Bratkovsky, J. Phys. C: Condens. Matter. **10**, L691 (1998).
24. M. Schluter, M. Lannoo, M. Needels, G.A. Baraff, and D. Tománek, Phys. Rev. Lett. **68**, 526 (1992).
25. J.-C. Charlier, X. Gonze, and J.-P. Michenaud, Europhys. Lett. **28**, 403 (1994); M.C. Schabel and J.L. Martins, Phys. Rev. B **46**, 7185 (1992).
26. F. Taddei, S. Sanvito, C.J. Lambert, J.H. Jefferson, Phys. Rev. Lett. **82**, 4938 (1999).
27. M. Büttiker, Y. Imry, R. Landauer, S. Pinhas, Phys. Rev. B **31**, 6207 (1985).
28. S. Sanvito, C.J. Lambert, J.H. Jefferson, to appear in Phys. Rev. B, and also cond-mat/9903381
29. C.J. Lambert, V.C. Hui, S.J. Robinson, J. Phys. C: Condens. Matter. **5**, 4187 (1993).